# Neutron star mechanics in the observers inertial frame

July 15, 2014

## 1 Introduction

In the rotating body frame we can solve Euler's rigid body equations to calculate the motion of the spin vector $\boldsymbol{\omega}$ as a function of time; this allows observation of precession without resolving individual rotations on the faster spin period. Observations of the star are made in the inertial frame and so observers report on quantities calculable from the phase: timing residuals, frequency of the the pulse and the spindown rate. In an effort to understand the implications of precession on these quantities we aim to calculate the motion of the star in the inertial frame. A natural way to do this is to determine the Euler angles which transform the rotating body frame axis, denoted by $(x', y', z')$, to the inertial frame axis for which we will use $(x, y, z)$. Using the Euler angle parameterisation as described by Landau and Lifshitz (1969) a schematic of how these angles are constructed is given in figure 1.1.

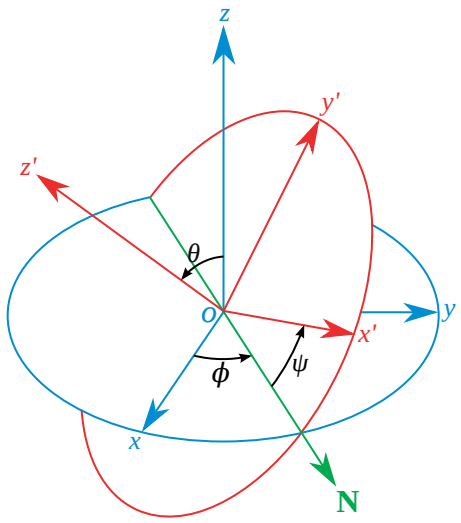


Figure 1.1: Schematic of the Euler angle rotation. In the inertial frame the angular momentum is set to lie initially along the $z$ axis. In the rotating body frame for a biaxial body the deformation lies along $z'$ while the spin vector initially lies along in the $x' - z'$ plane.

In the body frame we define the diagonal moment of inertia to have components $I_{xx}$, $I_{yy}$ and $I_{zz}$ and acted upon by a torque $\boldsymbol{T}$. The Euler rigid body equations are then the left most equations

in (1.1). Decomposing the motion of the spin vector into Euler angles and rearranging yields the second set of equations in (1.1) for the rate of change of the three Euler angles.

$$\begin{aligned}
\dot{\omega_x} &= \frac{1}{I_{xx}}\left[T_x + (I_{yy} - I_{zz})\,\omega_y\omega_z\right], & \dot{\theta} &= \omega_x\cos\psi - \omega_y\sin\psi, \\
\dot{\omega_y} &= \frac{1}{I_{yy}}\left[T_y + (I_{zz} - I_{xx})\,\omega_x\omega_z\right], & \dot{\phi} &= \frac{\omega_x\sin\psi + \omega_y\cos\psi}{\sin\theta}, \\
\dot{\omega_z} &= \frac{1}{I_{zz}}\left[T_z + (I_{xx} - I_{yy})\,\omega_x\omega_y\right], & \dot{\psi} &= \omega_z - \dot{\phi}\cos\theta,
\end{aligned} \tag{1.1}$$

These equations can be solved numerically using a time stepper[1]. The rotation period of the star is several orders of magnitude smaller than the precession period, as a result the Euler angles evolve on a much shorter time scale than the body frame spin components. This is numerically expensive. To allow efficient investigations we will therefore consider unrealistic values to understand the different types of motion before using realistic values only in cases of interest.

## 2 Initial conditions

Solving the rigid body equations in the body frame the following initial conditions are imposed on the spin vector:

$$\omega_x = \omega_0\sin(a_0), \qquad \omega_y = 0, \qquad \omega_z = \omega_0\cos(a_0), \tag{2.1}$$

such that $\boldsymbol{\omega}(t=0)$ lies in the $x'-z'$ plane. Defining the moment of inertia and torque this is sufficient to solve the rigid body equations. The angular momentum vector in the two frames are related by the rotation matrix $R(\theta,\phi,\psi)$ constructed from the Euler angles

$$\boldsymbol{J}|_{\mathrm{Rot}} = R(\theta,\phi,\psi)\;\boldsymbol{J}|_{\mathrm{In}} \tag{2.2}$$

The angular momentum in the inertial frame is given by $\boldsymbol{J}|_{\mathrm{Rot}} = I\boldsymbol{\omega}$, the initial conditions on $\boldsymbol{\omega}$ then provide initial conditions for the angular momentum. BY setting an initial condition on the angular momentum in the inertial frame we uniquely define the inital Euler angles. We are free to set the initial angular momentum in the inertial frame to lie along the inertial $z$ axis such that $\boldsymbol{J}_0|_{\mathrm{I}} = |J|\hat{z}$. In the torque free case this will remain true, the addition of the torque will induce variations. Normalising the two vectors in equation (2.2) and rearranging gives the expression

$$\begin{bmatrix} \sin\psi_0\sin\theta_0 \\ \sin\psi_0\cos\theta_0 \\ \cos\theta_0 \end{bmatrix} = \frac{1}{\sqrt{(I_{xx}\sin a_0)^2 + (I_{zz}\cos a_0)^2}} \begin{bmatrix} I_{xx}\sin a_0 \\ 0 \\ I_{zz}\cos a_0 \end{bmatrix}. \tag{2.3}$$

We have three equations for two unknowns; our choice to set $\boldsymbol{J}$ along the $z$ axis leaves the initial value of $\phi$ a free variable, for simplicity we set it to $\phi_0 = 0$. Inserting this and comparing the components

[1] For now we will use the rkf45 stepper provided by GSL

$$\theta_0 = \arccos\left(\frac{I_{zz}\cos a_0}{\sqrt{(I_{xx}\sin a_0)^2 + (I_{zz}\cos a_0)^2}}\right). \tag{2.4}$$

For $\psi_0$, we use that $\sin(\arccos(x)) = \sqrt{1-x^2}$ giving:

$$\psi_0 = \frac{\pi}{2}. \tag{2.5}$$

We now have a suitable set of initial conditions to solve the 6 ODEs in (1.1).

# 3 Biaxial body with no torque

This system was studied by Jones and Andersson (2001) where it was found that the angular momentum $\boldsymbol{J}$, deformation axis $\hat{\boldsymbol{n}}_d$[2] and spin vector $\boldsymbol{\omega}$ are always coplanar. We will label this plane as the reference plane. Decomposing the angular velocity according to

$$\boldsymbol{\omega} = \dot{\phi}\hat{\boldsymbol{n}}_J + \dot{\psi}\hat{\boldsymbol{n}}_d \tag{3.1}$$

it was found that $\phi$ monotonically increases at the fast spin frequency whilst $\psi$ decreases at the slower precession frequency whilst $\theta$ should remain constant.

Numerically solving the equations of motion these results are confirmed in figure 3.1(b) and also demonstrate the usual free precession in the body frame in 3.1(b): the azimuthal angle $\varphi$ monotonically increases whilst the polar angle $a$ and the spin magnitude $\omega$ remain fixed.

It is of note that in these simulations $\theta$ is not constant, this is caused by the finite numerical precision when calculating the subtraction defined in equation (1.1) for $\dot{\theta} = 0$. On short time scales these errors have fractional size $1 \times 10^{-14}$ and so the results hold. Over sufficiently long time scale these errors can accumulate and eventually leads to a complete loss of numerical accuracy, we must therefore be vigilant to ensure this does not occur when considering realistic values.

[2]for a biaxial body we set $\hat{\boldsymbol{n}}_d$ to lie along the $z'$ axis of the body frame

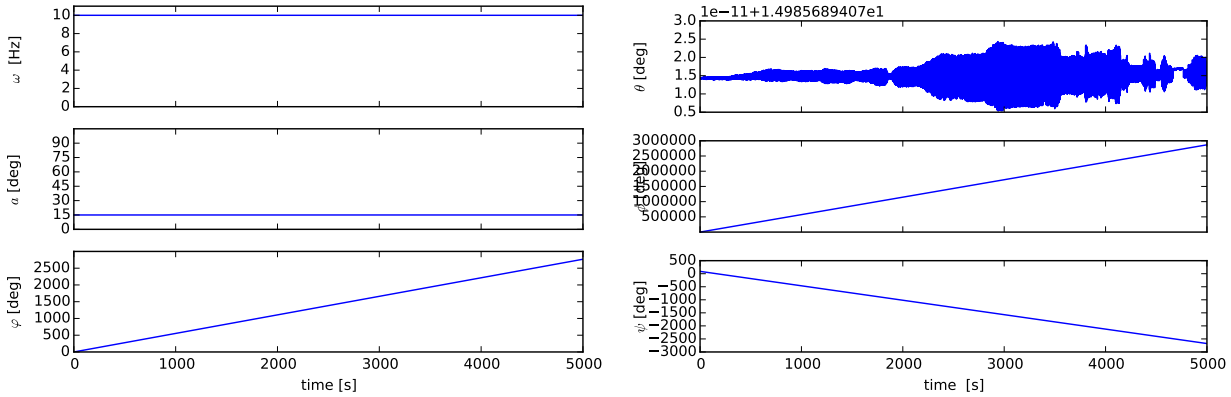


**(a)** Spherical components in the body frame

**(b)** Euler angles

Figure 3.1: Solution to the differential equations in (1.1) for a biaxial body with deformation of $\epsilon_{I3} = 1 \times 10^{-3}$

## 3.1 Physical observables

Having the Euler angles allows us to transform from the rotating frame into the inertial frame of an exterior observer. We observe pulsars from the electromagnetic radiation that streams out along open field lines, while the mechanism is poorly understood in this model we will assume a thin columnated beam is emitted along the magnetic dipole $\hat{\boldsymbol{m}}$. In the body frame we set $\hat{\boldsymbol{m}}$ at an angle $\chi$ to the $z'$ axis with unit vector $[\sin(\chi), 0, \cos(\chi)]$. Using the Euler angles to rotate this unit vector, the components in the inertial frame are given by:

$$\hat{\boldsymbol{m}} = \begin{bmatrix} \cos\phi\cos\psi\sin\chi - \sin\phi\cos\theta\sin\psi\sin\chi + \sin\phi\sin\theta\cos\chi \\ \sin\phi\cos\psi\sin\chi + \cos\phi\cos\theta\sin\psi\sin\chi - \cos\phi\sin\theta\cos\chi \\ \sin\theta\cos\psi\sin\chi + \cos\theta\cos\chi \end{bmatrix}. \tag{3.2}$$

Following the work of Jones and Andersson (2001) two angles $\Phi$ and $\Theta$ are defined to describe the polar and azimuth of $\hat{\boldsymbol{m}}$ in the inertial frame. Defining $\Phi = \arctan(\hat{\boldsymbol{m}}_y/\hat{\boldsymbol{m}}_x)$ after some algebra we arrive at:

$$\Phi = \phi - \frac{\pi}{2} + \arctan\left(\frac{1}{\cos\theta}\left(\frac{\cos\psi\tan\chi}{\tan\theta - \sin\psi\tan\chi}\right)\right), \tag{3.3}$$

while the polar angle of the magnetic dipole is given by:

$$\Theta = \arccos(\hat{\boldsymbol{m}}_z) = \arccos(\sin\theta\sin\psi\sin\chi + \cos\theta\cos\chi) \tag{3.4}$$

**Instantaneous electromagnetic frequency** An observer sees a pulse every time the magnetic dipole passes over them, making a simplification that a pulse is observed everytime the magnetic dipole cuts the plane containing the observer and the angular momentum vector $\boldsymbol{J}$. In effect we say the observer sees a pulse when the azimuth $\Phi$ is equal to their own regardless of the polar angle $\Theta$. In this way $\Phi$ gives the phase of the signal for an observer at $\Phi = 0$ and $\Theta$ defines the amplitude being maximum when equal to that of the observer (who we place at $\Theta = 0$) . Taking a derivative

of the phase:

$$\dot{\Phi} = \dot{\phi} + \frac{\sin\chi\left(\dot{\psi}(\cos\theta\sin\chi - \sin\psi\sin\theta\cos\chi) + \dot{\theta}\cos\psi(\cos\theta\sin\chi - \sin\psi\sin\theta\cos\chi)\right)}{(\sin\theta\cos\chi - \cos\theta\sin\psi\sin\chi)^2 + \cos^2\psi\sin^2\chi}. \tag{3.5}$$

This is then the *instantaneous electromagnetic frequency*, an observer will measure the time averaged value of $\dot{\Phi}$ as the 'spin frequency' of the star Note that this result is an extension of equation (43) from Jones and Andersson (2001) treating $\theta$ as a function of time instead of a constant. Jones et al. demonstrated that two distinct behaviours exist for the time average of equation (3.5). The two cases are catergoried by $\theta > \chi$ or $\theta < \chi$; recall that for the biaxial star with no torque $\theta \approx a_0$.

## 3.2 Understanding the two cases

To get a feeling for the mechanics we consider the decomposition of the angular velocity in equation 3.1 into rotations about $\hat{\boldsymbol{n}}_J$ and $\hat{\boldsymbol{n}}_d$. Any vector (such as $\hat{\boldsymbol{m}}$) in the body frame can be understood in the inertial frame as undergoing two motions: keeping $\phi$ fixed and increasing $\psi$ rotates the vector in a cone aboout the $\hat{\boldsymbol{n}}_d$ axis, holding instead $\psi$ fixed and increasing $\phi$ sweeps the vector about a cone centered around the $\hat{\boldsymbol{n}}_J$ axis. Calling these cones the precession and spin cones respectively the resulting motion can be understood as the superposition of the two. In figure 3.2 an illustration is given of these cones projected into the reference plane for the three orderings of $\theta$ and $\chi$.

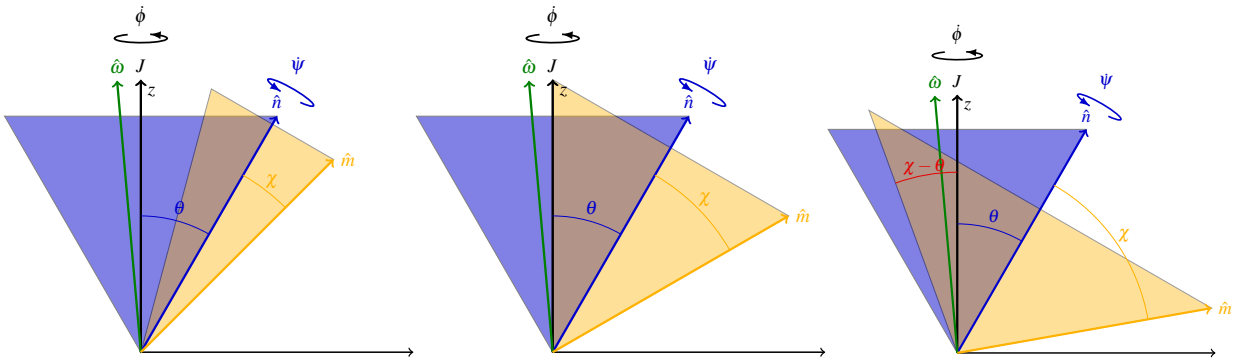


**(a)** $\theta > \chi$ **(b)** $\theta = \chi$ **(c)** $\theta < \chi$

Figure 3.2: Diagrams depiciting 2D projections of the cones swept out by the different motions under torque free precession onto the reference plane. The yellow cone is that swept out by $\hat{\boldsymbol{m}}$ about $\hat{\boldsymbol{n}}_d$ at the slow precession frequency; the blue cone is that swept out by $\hat{\boldsymbol{n}}_d$ about $\boldsymbol{J}$ at the fast spin frequency. It should be noted that the precession cone rotates in the opposing direction to the spin cone for oblate bodies.

The motion of the magnetic dipole about the precession cone evolves on a much longer timescale than its motion about the spin cone, as a result the star will always pulsate once every spin period, but the long precession will induce variations. Because of the large difference in timescales the motion of $\hat{\boldsymbol{m}}$ can be considered as the slow evolution of a third cone swept out by $\hat{\boldsymbol{m}}$ about $\boldsymbol{J}$ which we will call the dipole cone. The half angle made by this cone is exactly the azimuthal angle $\Theta$ calculated in equation (3.4); the frequency with which $\hat{\boldsymbol{m}}$ rotates in the dipole cone is given by

equation (3.5), both these quantities will vary on the precession time scale. In figures 3.3(a) and (b) the frequency and polar angle variations are plotted for three particular cases, with reference to these plots we now discuss the three cases:

- The $\chi = \theta/2$ case: The precession cone is narrow and does not extend over the angular momentum vector. The polar angle $\Theta$ of the dipole cone then oscillates sinusoidally between $\theta + \chi$ and $\theta - \chi$ during a precession cycle. The spin frequency $\dot{\Phi}$ has an average value of $\dot{\phi}$[3] and oscillates about this value, comparing with the $\Theta$ variations demonstrates these oscillations are locked in phase with the rotation of $\hat{\boldsymbol{m}}$ in the precession cone. Recalling that the precession cone counter rotates with respect to the spin cone, at $\theta+\chi$ the precession cone motion acts in the opposing direction to the spin cone, this causes a reduction in the spin frequency away from the average; by contrast at $\theta + \chi$ the counter rotation is now in favour of the spin frequency and as a result the spin frequency is increased above the average.

- The $\chi = \theta$ case: Here the angular momentum vector sits exactly on the precession cone, this suggest $\hat{\boldsymbol{m}}$ can align exactly with the angular momentum. When this happens the spin frequency tends to zero (due to numerical error this never actually occurs) manifesting as sharp dips in the spin frequency; at the same time the polar angle tends to zero.

- The $\chi = 4\theta$ case: The precession cone now extends over the angular momentum vector, this means it always acts to reduce the spin frequency; as a result the the spin frequency has an average value of $\dot{\phi}+\dot{\psi}$. The polar angle can vary between $\theta+\chi$ and $\chi-\theta$, for $\chi$ close to $\theta$ the deviations away from the average are large while as $\chi$ increases the deviations get smaller as thehalf angle of the dipole cone increases.

[3]See Jones 2001 for a detailed explanation

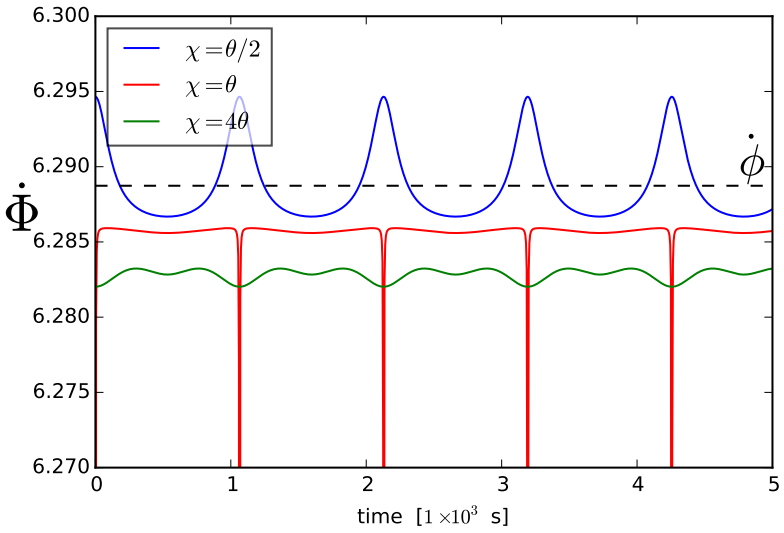


**(a)** Variations in the spin frequency

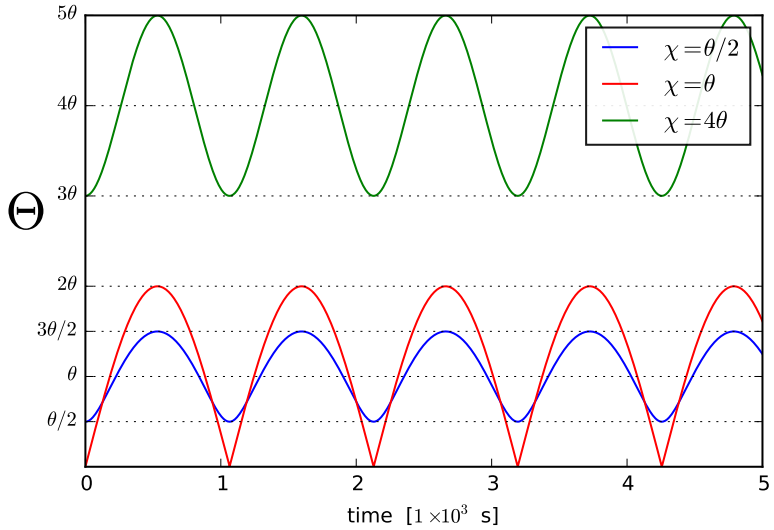


**(b)** Variations in polar angle

Figure 3.3

### 3.2.1 Timing residuals

The principle indicator that a spin down power law does not accurately describe the evolution of pulsars is the coherent structure which exists in the timing residuals. We now aim to introduce the tools required to calculate the timing residuals from our model and determine what effect, if any, torque free precession will induce.

Starting with the instantaneous electromagnetic frequency as given by equation (3.5) and nu-

merically integrating yields the phase of the pulse, we will label this $\Phi_{\text{exact}}$, a quadratic polynomial is then fitted to this phase using a least squares method. The resulting coefficients, $\dot{\nu}, \nu$ and $\phi_0$ are the physical quantities best describing the results for a power law spin down. Calculating the phase according to this polynomial gives $\Phi_{\text{fit}}$ the fitted phase. The difference between these two phases is the timing residual as calculated by observers.

In figure 3.4 we plot the timing residuals as calculated in the torque free model while changing the inclination of the magnetic dipole. It is worth noting that there is an issue in doing this, namely the power law spin down assumes that the star is in fact spinning down; without the torque this model will not spin down. We can however interpret these results as the effect of precession on timing residuals in the limit for which the variation due to precession is much stronger than the spin down.

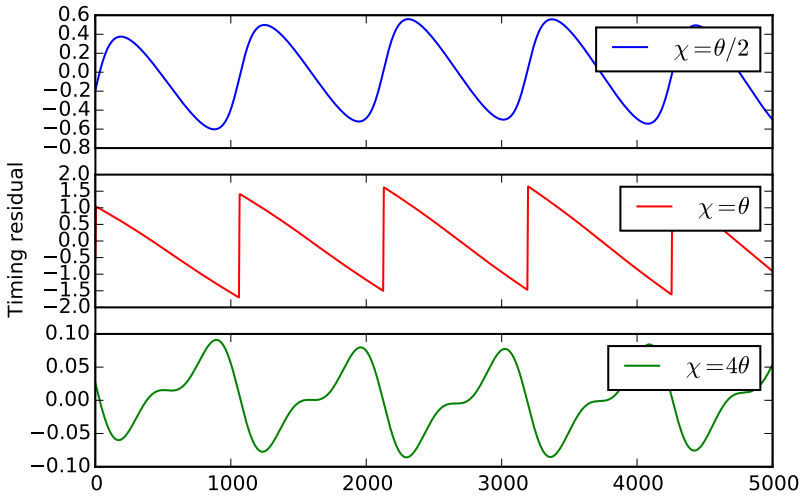


Figure 3.4: Plot of the timing residuals for various angles of $\chi$ in the torque free model.

The results show that the precession will induce a sinusoidal variation on the precession timescale, the magnitude is proportional to the angle $\chi$, there will also be a dependence on the initial angle $a_0$ as this is a geometric effect.

## 3.3 Slowdown Rate $\dot{\nu}$

The second observable which is often considered in characterising periodic patterns in pulsar signals is the slowdown rate. In this simple model the slowdown rate is given by $\ddot{\Phi}$, however calculating an analytic expression is highly non-trivial, although theoretically possible. Instead of relying on computational aids to achieve this we instead turn to the method prescribed by Lyne et al. (2010): selecting short sections of data of length $T$ a quadratic is fitted allowing an estimation of $\dot{\nu}$, this process is repeated every $\sim T/4$ through the data set. We choose $T$ such that it is a fraction of the precession period over which we expect quantities to be modulated. To aid the eye the values have been normalised and plotted in figure 4.4. This has the advantage that any features resulting from the technique will also be picked up.

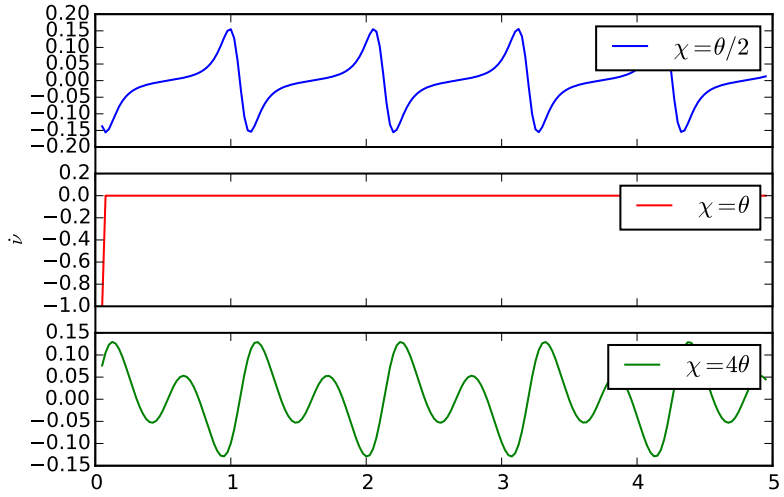


Figure 3.5: Slow down rate

# 4 Biaxial body with torque

The torque which produce the observed electromagnetic radiation will play an important role in determining the time variability of the observed pulse on earth. The torque is modelled as a magnetic dipole, denoted by $\hat{\boldsymbol{m}}$, frozen into the star at an angle $\chi$ to the $z'$ axis in the $x' - z'$ plane. Following the work of Deutsch (1955), the torque is presented here in form found in Goldreich (1970).

$$\boldsymbol{T} = \frac{2R}{3c} I_0 \epsilon_A \omega^2 (\boldsymbol{\omega} \times \hat{\boldsymbol{m}}) \times \hat{\boldsymbol{m}} + \epsilon_A I_0 (\boldsymbol{\omega} \cdot \hat{\boldsymbol{m}})(\boldsymbol{\omega} \times \hat{\boldsymbol{m}}), \qquad \text{with} \qquad \epsilon_A = \frac{m^2}{I_0 R_6 c^2}, \tag{4.1}$$

where $\boldsymbol{\omega}$ is the spin vector and $\epsilon_A$ is the magnetic deformation (see Glampedakis and Jones, 2010). The first term on the right hand side is often referred to as the *spin down*, or *braking* torque. As this suggests it is responsible for the power law retardation of spin frequency and has an associated timescale $\tau_S$. The second term is known as the *anomalous* torque which acts on a timescale $\tau_A$. Inserting this torque into the ODEs defined in (1.1) then we have three time scales: the two due to the torque stated above and the precession time scale $\tau_P$ as found by Jones and Andersson (2001). These three timescales are given by:

$$\tau_P = \frac{1}{\epsilon_I \nu_0}, \qquad \tau_A = \frac{1}{\epsilon_A \nu_0}, \qquad \tau_S = \frac{3c}{2R} \frac{1}{\epsilon_A \nu_0^2}, \tag{4.2}$$

where $\nu_0$ is the initial spin frequency and $\epsilon_I$ is the magnitude of the elastic deformation along $z$ ($I_{zz} = I_{xx} + \epsilon_I$). In previous work we have shown that realistic pulsars exist in the region $\tau_P > \tau_A$ for which $\epsilon_A < \epsilon_I$, in order to demonstrate the effect of the torque we will work for $\epsilon_A = \epsilon_I/2$.

## 4.1 Results

In figure 4.1 we plot the spherical components of the spin vector in the body frame (a), and the evolution of the Euler angles. Comparing this with figure 3.1 the most striking difference is the

wobble in both $\theta$ and $a$, on closer inspection one also finds this wobble in the other angles and the magnitude of $\boldsymbol{\omega}$ along with a monotonic spin down.

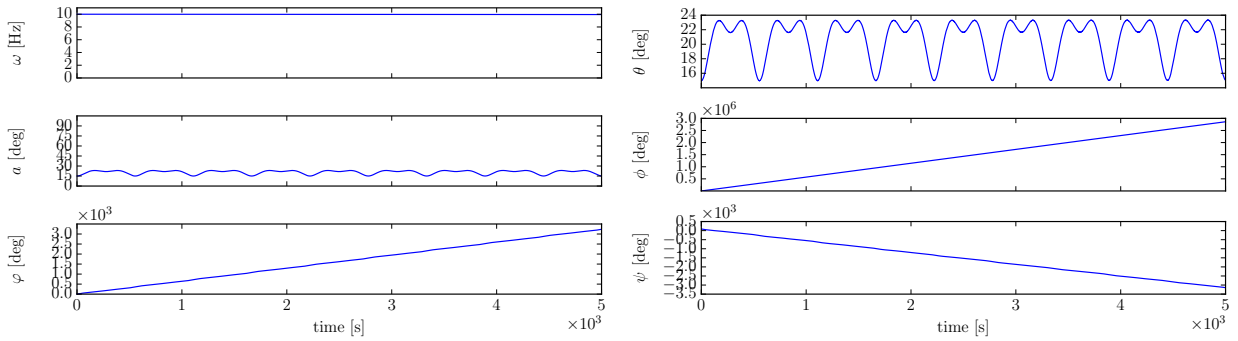


**(a)** **(b)**

Figure 4.1: Solution to the differential equations in (1.1) including the torque defined in (4.1) for a biaxial body with $\epsilon_A = \epsilon_I/2$

## 4.2 Observables

In figure 4.2 we reproduce plots of figure 3.3 with the addition of the torque. The torque introduces two additional effects: $\dot{\Phi}$ the instantaneous electromagnetic frequency decays slowly, this is caused by the spin down torque and is full agreement with what we expect; a fast sinusoidal oscillation in $\dot{\Phi}$ on the spin time scale, observable as a broadening of the line, is a result of the anomalous torque. As for the polar angle $\Theta$ the anomalous torque causes slight changes in the limits of the sinusoidal variation. Both the anomalous torque effects can be understood by realising that this effectively adds a triaxiality into the moment of inertia tensor.

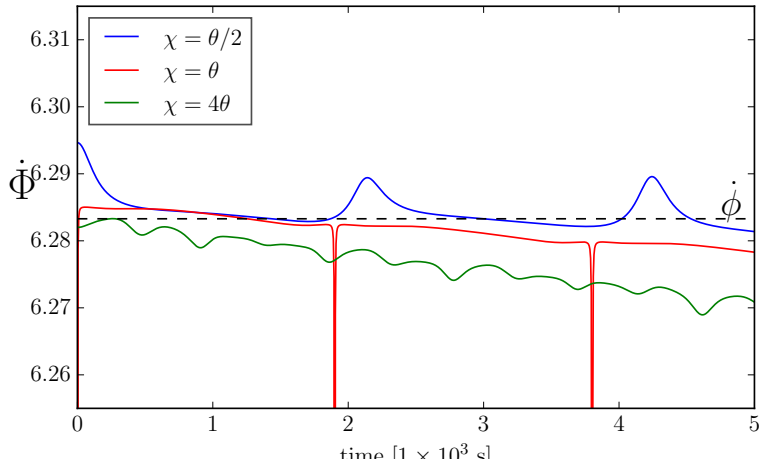


**(a)** Variations in the spin frequency

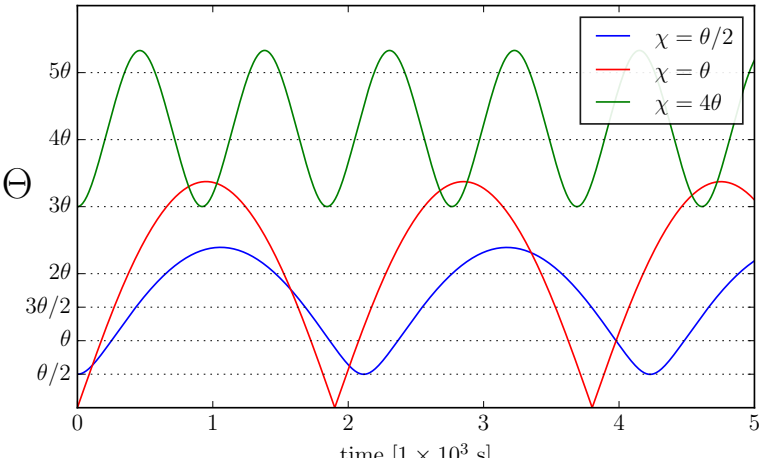


**(b)** Variations in polar angle

Figure 4.2

### 4.2.1 Timing residual

Including the torque the timing residuals are plotted in figure 4.3, while the sinusoidal variation remains the magnetic inclination varies the spin down rate and hence the period of the these variations.

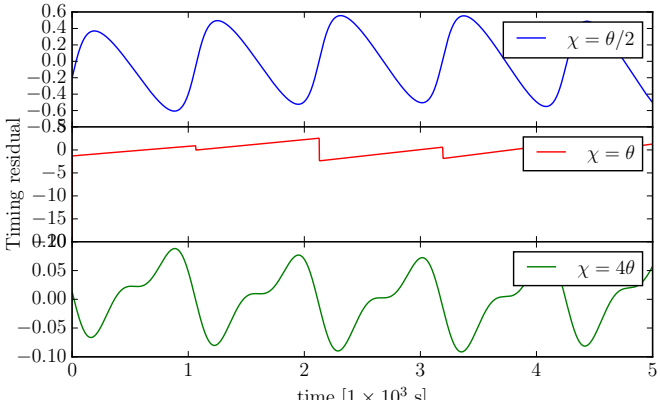


**(a)** No anomalous torque

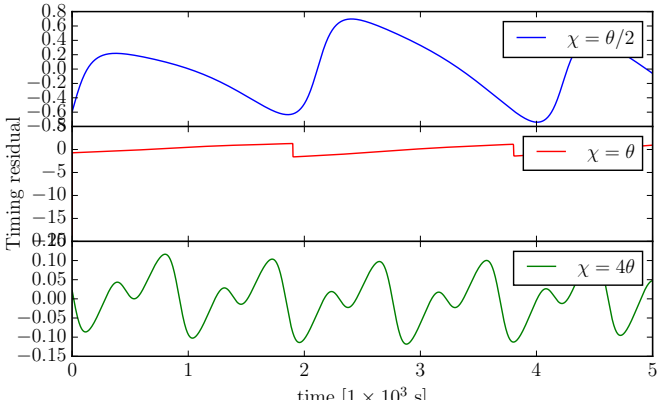


**(b)** With anomalous torque

Figure 4.3: Plot of the timing residuals for various angles of $\chi$ including the effects of the torque.

## 4.3 Slowdown Rate $\dot{\nu}$

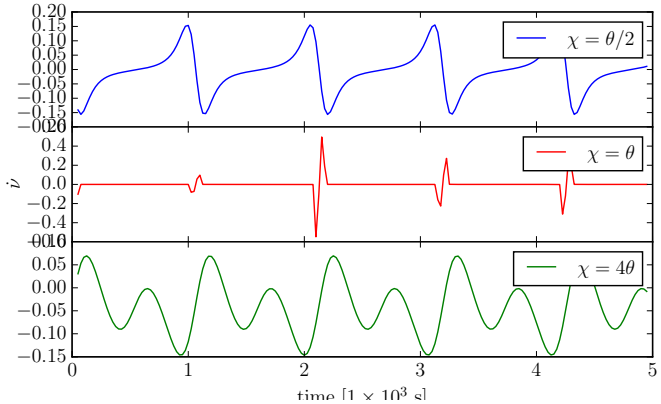


**(a)** No anomalous torque

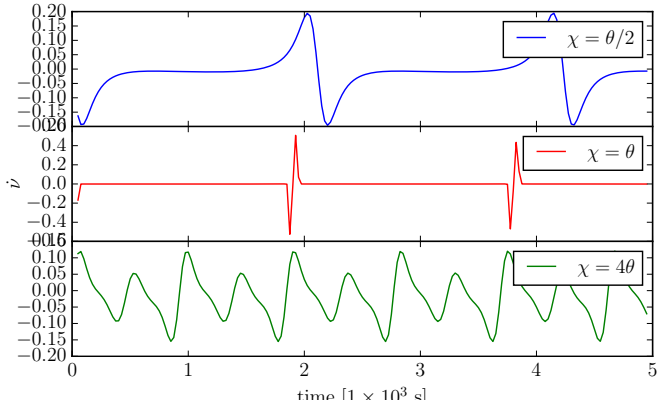


**(b)** With anomalous torque

Figure 4.4

# 5 B1828-11

In order to compare the prediction of our model with actual observations we select the pulsar B1828-11. There is some evidence in work by Lyne et al. (2000) that this pulsar undergoes precession, and work by Hobbs et al. (2010) and Lyne et al. (2010) documents the timing residuals and spin down rate with unsurpassed accuracy. This makes the pulsar ideal for study under the assumption that the variations are caused by precession.

From table 1 in Lyne et al. (2000) we have that B1828-11 has a spin period of $P_0 = 405$ms. We can calculate the magnetic deformation using the surface magnetic field

$$\epsilon_A = \frac{m^2}{I_0 R c^2} = \frac{(\frac{1}{2} B_s R^3)^2}{I_0 R c^2} \tag{5.1}$$

From table1 we have that $B_s = 5 \times 10^{12}$G and using canonical values of $R$, $c$ and $I_0$[4] yields $\epsilon_A = 6.94 \times 10^{-12}$.

[4]Should I give the actual values?

For the elastic deformations we have an upper limit from gravitational wave searches of $1 \times 10^{-6}$. We now make the assumption that it is precession which causes the variations in signal, from Jones and Andersson (2001) we may therefore use that

$$\epsilon_I \sim \frac{P_{\rm spin}}{P_{\rm precession}} \tag{5.2}$$

Lyne found timescales of 1000, 500 and 250 days for the variations, we will use the shortest of these such that $P_{precession} = 250$ days. Hence we have an elastic deformations of $1.88 \times 10^{-8}$. This also agrees well with Lyne et al. (2010) B1812-11 is observed for $\sim$ 6000 days during which 22 oscillations occur, this gives a period of about 273 days. With these values we have the following timescales

$$\tau_S = 1.06 \times 10^{15} \text{ s} \qquad \tau_A = 5.83 \times 10^{10} \text{ s} \qquad \tau_P = 3.55 \times 10^{6} \text{ s}$$

No obvious way exists to define $\chi$ other than to assume it must not be aligned on grounds that we can observe the pulsar. Since this pulsar satisfies the region A conditions and is therefore subject to the critical of $\chi$ we again choose the two values of $\chi$ previously used.

# 6 Torque switching effects

Lyne et al. (2010) found strong evidence that a periodic switching in the rate of spin down $\dot{\nu}$ induces structure in the residual. Modeling this they found that for a strictly periodic switching the variations are precisely mirrored in the residual, if instead a random dither is introduced between switches the residuals take form very similar to those found in Hobbs et al. (2010). The model assumes apriori that the switching occurs with a time scale of several 100 days, the switching itself is motivated by changes in the magnetosphere: enhances emmison correlates with larger values of $\dot{\nu}$. A mechanism is required to keep the magnetosphere in serveral meta-stable states with swithing occuring on a much shorter time scale than the period between swithces. **?** proposed that if the star were to be precessing, its relative orientation to the angular momentum may bias it towards different magneospheric configurations. Stars born near the boundary between configurations will then periodially flip between them on the precession timescale which matches well with the observed switching times. In this section we aim to model this proposal by extending our model; this is done by adding a switching into the torque that depends on the angle $\Psi$ between $\hat{\boldsymbol{m}}$ and the angular momentum. We define the sw

As previously shown this angle is bounded by $|\chi - \theta| < \Psi < \chi + \theta$ during a precessional cycle, it therefore has an average value of $\Psi_{\rm ave} \max(\theta, \chi)$; while many different scenarios could be considered we choose the following:

$$\boldsymbol{S}(\Psi, \chi, \theta, \upsilon) = \begin{cases} 1 & \text{if} \quad \Psi > \Psi_{\rm ave} \\ 1 - \upsilon & \text{else} \end{cases} \tag{6.1}$$

where $\upsilon$ is a number between 0 and 1 parameterising the reduction in torque.

# 7 Pulse amplitude and width

We now have a model for the evolution of the magnetic dipole $\hat{\boldsymbol{m}}$ in the inertial frame described by its angular components $\Theta$ and $\Phi$. We can now calculate the pulse amplitude as observed at $\Phi_O, \Theta_O$

by modelling the emmision region by a two dimensional Gaussian:

$$A(\Phi,\Theta) = A_0 \exp\left(-\frac{(\mod_{2\pi}(\Phi)-\Phi_O)^2}{2\sigma_\Phi^2} - \frac{(\mod_{2\pi}(\Theta)-\Theta_O)^2}{2\sigma_\Theta^2}\right) \tag{7.1}$$

Taking a given numerical solution to the original ODEs and computing the angles $\Phi$ and $\Theta$ as a function of time then insering these into this expression gives the amplitude of the pulse as seen by the observer.

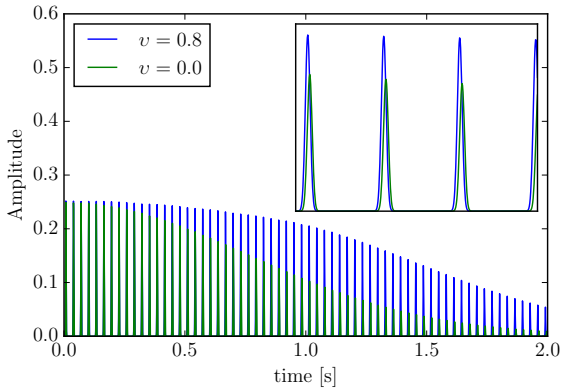


Figure 7.1

**Pulse width** To measure the pulse width the data is dividided into sections short enough that free precession modulation effects are negligible. The pulses are then assumed to be approximately Gaussian such that they can be described by

$$g(t) = ae^{-(t-b)^2/c^2} \tag{7.2}$$

The full width at half maximum, or equivalently $W_{50}$ is then given by $W_{50} = c\sqrt{\ln 2}$. To measure $c$ for a single pulse we can integrate

$$\int_{-\infty}^{\infty} ae^{-(t-b)^2/c^2} dt = a|c|\sqrt{\pi}. \tag{7.3}$$

If we then numerically integrate over $n$ pulses provided each pulse falls off sufficiently quickly then we have

$$|c| = \frac{\int_{T_{\text{obs}}} A(t)dt}{na\sqrt{\pi}} \tag{7.4}$$

Where $A(t)$ is the pulse amplitude over the observation time as calculted in equation (7.1). To implement this over an arbitary observation time requires the calculation of the number of pulses and there amplitude $a$. The result of a particular example is given in figure 7.2

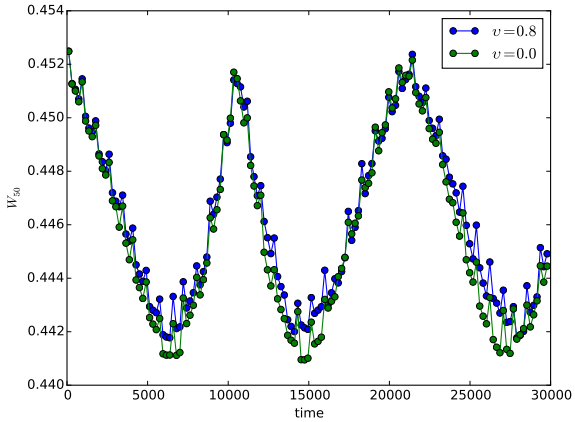


Figure 7.2

## References

Deutsch, A. (1955). The electromagnetic field of an idealized star in rigid rotation in vacuo. *Annales d'Astrophysique*.

Glampedakis, K. and Jones, D. I. (2010). Implications of magnetar non-precession. *Monthly Notices of the Royal Astronomical Society: Letters*, 405(1):L6–L10.

Goldreich, P. (1970). Neutron star crusts and alignment of magnetic axes in pulsars. *The Astrophysical Journal*.

Hobbs, G., Lyne, a. G., and Kramer, M. (2010). An analysis of the timing irregularities for 366 pulsars. *Monthly Notices of the Royal Astronomical Society*, 402(2):1027–1048.

Jones, D. I. and Andersson, N. (2001). Freely precessing neutron stars: model and observations. *Monthly Notices of the Royal Astronomical Society*, 324(4):811–824.

Landau, L. D. and Lifshitz, E. M. (1969). *Mechanics*. Pergamon press.

Lyne, A., Hobbs, G., Kramer, M., Stairs, I., and Stappers, B. (2010). Switched Magnetospheric Regulation of Pulsar Spin-Down. *Science*, 329:408–.

Lyne, A. G., Stairs, I. H., and Shemar, S. L. (2000). Periodicities in Rotation and Pulse Shape in PSR B1828-11. In Kramer, M., Wex, N., and Wielebinski, R., editors, *IAU Colloq. 177: Pulsar Astronomy - 2000 and Beyond*, volume 202 of *Astronomical Society of the Pacific Conference Series*, page 93.